

BIODYNAMIC PILOT MODELLING FOR AEROELASTIC A/RPC

Pierangelo Masarati, Giuseppe Quaranta

pierangelo.masarati@polimi.it, giuseppe.quaranta@polimi.it

Politecnico di Milano, Italy

Larisa Zaichik, Yuri Yashin, Pavel Desyatnik

zaichik@tsagi.ru, yuyashin@yandex.ru, desiatnik_pavel@mail.ru

TsAGI, Russia

Marilena D. Pavel, Joost Venrooij

m.d.pavel@tudelft.nl, j.venrooij@tudelft.nl

TU Delft, The Netherlands

Hafid Smaili

hafid.smaili@nlr.nl

NLR, The Netherlands

Abstract

This work discusses the identification and the modeling of the biomechanics of fixed and rotary wing aircraft. The study is conducted within the European Commission 7th Framework Programme 'Aristotel' to understand the potential impact of involuntary pilot activity on the stability and the handling qualities of the vehicle, and to develop the capability to assess the proneness of the vehicle to adverse aircraft and rotorcraft pilot couplings. Transfer function identification from experimental results and multibody modeling of pilot biomechanics are used to provide an insight into the problem and to devise quantitative results that can be used in coupled bioaeroservoelastic analysis. Their application to stability assessment is discussed, and a novel criterion to estimate handling quality degradation as a consequence of adverse aircraft pilot coupling is outlined.

1 INTRODUCTION

The study of Biodynamic Feedthrough (BDFT) in relation with fixed-wing aircraft dates back to the late 1960s; in [1, 2], a detailed and accurate study of the neuromuscular implications in the pilot-vehicle interaction was presented. In [3], a sophisticated although linear model of the torso and of the hand was used to analyze feedthrough of a semisupine pilot, in view of the design of advanced man-machine interfaces for high-performance aircraft (a sidestick with elbow rest support). In [4], the problem of aircraft roll ratcheting, an "unwanted and inadvertent high frequency oscillation in the roll axis encountered in high performance fighter aircraft during rapid roll maneuvers," was analyzed using a model of the hip, the torso and the arm of the pilot, connected by linear springs and dampers, whose characteristics were obtained by fitting the experimental frequency response of actual pilots. These, as well as other models proposed in the literature, are essentially linear, with equivalent stiffness and damping properties obtained by fitting experimental data. In [4] it is reported that good correlation with experimental data could only be obtained using an unrealistic value for the mass of the arm.

BDFT is task dependent, as indicated in [5], where the problem was experimentally investigated in rela-

tion with fixed-wing aircraft control inceptors. BDFT experiments related to the collective control lever have been conducted in [6–8]. They highlighted significant variability associated with the size of the human subject and posture. For example, in [6] Mayo divides the subjects in two groups: 'ectomorphic', individuals of small and lean build, and 'mesomorphic', subjects of large bone structure and muscle build. In [6] a generic dependence of BDFT magnitude on control inceptor reference position was proposed; in [8], the characteristic poles of the BDFT transfer function varied significantly in frequency and damping with the reference position of the control.

This paper illustrates the activity on pilot biomechanics that was performed within the European Commission 7th Framework Programme project ARISTOTEL¹ on aircraft and rotorcraft pilot couplings — tools and techniques for alleviation and detection. The aim and scope of the project is discussed in detail in [9, 10]. A detailed review on aircraft and rotorcraft-pilot interaction is presented in [11]. This work specifically addresses the experimental and numerical investigation of pilot biomechanics, which affects the involuntary action of the pilot on the vehicle as a consequence of feeding the motion of the cockpit into the flight controls, modified in amplitude and phase by the

¹<http://www.aristotel.progressima.eu/>

passive dynamics of the pilot's body. The related experimental activity is presented in the companion paper [12], whereas the numerical investigation of the aeroelastic effects is discussed in [13]. First the transfer function approach is discussed. It is used to identify the unintentional behavior of the pilot with respect to specific axes, namely the collective and the lateral cyclic controls for helicopter cockpits of conventional design, and conventional wheel and center and side stick for fixed wing aircraft. Then an original multi-body approach to the detailed modeling of the biomechanics of the pilot's upper limbs is presented. Finally, the application of the biomechanical models to aeroservoelastic analysis of vehicle-pilot interaction is discussed.

2 TRANSFER FUNCTION APPROACH

2.1 Methodology

This work discusses BDFT within fixed and rotary wing aircraft and the pilot. A considerable amount of literature is available in the field of fixed wing aircraft, whereas the literature is somewhat scarce in the helicopter field.

Existing aircraft-pilot coupling (APC) criteria for fixed-wing aircraft do not practically take into account inceptor feel system characteristics, though their effects can be considerable. In Russia, early investigations revealed that APC tendencies of flexible transport aircraft can be attributed to a resonant peak in the pilot's neuromuscular system frequency response at 2–3 Hz [14].

With respect to rotorcraft, activity in this area was performed within the GARTEUR Helicopter Action Group 16 (HC AG-16) [7, 15–17] and continued within the European Commission Seventh Framework Programme ARISTOTEL [10].

The two types of vehicles share the layout of the central stick control inceptor ("Cyclic" in Fig. 1), which is used for ailerons/elevator in fixed wing aircraft and for cyclic pitch control in helicopters. Alternative layouts for fixed wing controls include the conventional wheel and the sidestick. The latter is being considered also for advanced rotorcraft (for example, the Sikorsky X2 experimental compound aircraft with stiff coaxial rotor). Lateral cyclic controls as well as aileron controls produce a roll rotation of the vehicle that is in accordance with the motion of the control inceptor. As a consequence, the motion of the inceptor produces a moment about an axis directly associated with the motion of the control, creating potential for unintentional coupling.

Among typical helicopter cockpit layouts, the collec-

tive control lever is specific of helicopters ("Collective" in Fig. 1). The lever is usually connected to the cabin floor by a revolute hinge aligned with the pitch axis, and held by the pilot's left hand. Pulling it upwards increases the collective pitch of the main rotor blades, increasing the main rotor thrust. As a consequence, the vertical motion of the hand produces vertical force, creating potential for unintentional coupling as well.

Pedals, also common to both aircraft types, are not considered in this work.

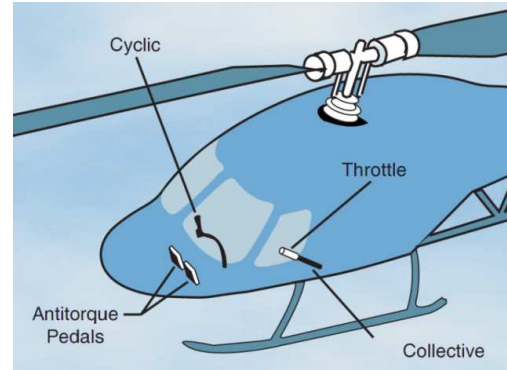


Figure 1: Helicopter control inceptors (from [18]).

The main research question considered in the "fixed-wing" experiments conducted within ARISTOTEL in PSPK-102 (TsAGI) and GRACE (NLR) flight simulators was to determine the effects of the inceptor type (traditional wheel, center stick and side stick) and its feel system characteristics (spring gradient, damping, breakout force, friction) on pilot-aircraft interaction. All the inceptors were loaded by the electrical loading system, which allows flexible changing of feel system characteristics. The human pilots were instructed to keep the inceptor in the vicinity of the reference position against lateral accelerations produced by flight simulator motion system. In experiments, the describing functions of the biodynamical pilot model were determined using Fast Fourier Transform:

$$(1) \quad \frac{\delta_s}{a} = \frac{S_{a-\delta_s}(j\omega)}{S_{a-a}(j\omega)}$$

where δ_s is the stick displacement; a is the acceleration produced by the motion of the platform.

With respect to helicopter BDFT, several tests have been conducted in the HELIFLIGHT full motion flight simulator at University of Liverpool (UoL) to identify helicopter pilots' biodynamic response when subjected to vertical and lateral accelerations. During these tests the flight simulator was used as a "shaker" for humans; the motion induced in the control inceptors by the oscillations imposed to the cockpit was measured, along with the motion induced in the limbs.

The excitations consisted of colored noise signals, band-pass filtered between 1 and 10 Hz, with zero mean and 0.004 g RMS (99.96% amplitude within 0.01 g). Excitation was applied in the vertical and lateral direction. During these tests, no specific flight task was required; the occupants were required to hold the control inceptors without compensating the stick vibration besides avoiding excessive drift. Transfer functions referred to a condition of 50% stroke for the collective lever and centred position for the cyclic control have been identified. Seven subjects were tested amongst the investigators, including three professional test pilots.

Transfer functions were identified using acceleration at the motion base of the flight simulator as input. Acceleration measured at the pilot hand holding the stick, acquired using a X-Sens MTi sensor, and stick position recorded by the flight simulator were used as output.

Collective control BDFT was measured using vertical acceleration as input, whereas lateral cyclic control BDFT was measured using lateral acceleration as input. Cross effects have not been considered. Measured data have been band-pass filtered using an optimal Butterworth filter with a pass band of 0.5–12 Hz. Good coherence between input and output was found in the band of interest for most of the measurements.

For such measurements the Blackman-Tukey algorithm [19] has been used to estimate the frequency response. Then, the frequency response were fitted using a rational polynomial model of the class

$$(2) \quad y(s) = \frac{A(s)}{B(s)}u(s) + e(s)$$

with appropriate numerator and denominator order.

2.2 Helicopter: Collective Control Device

Figure 2 summarizes the frequency response obtained in the collective inceptor case. Hand accelerations were used, since the coherence between the input and the inceptor rotation was too low in most cases. Key results are:

- there are significantly damped biodynamic poles in the 3–10 Hz range;
- transfer functions are well approximated using 5th or 6th order polynomials;
- BDFT shows high variability; transfer functions change significantly between different test pilots and between different tests for the same pilot;
- the identification procedures led to good correlation between predicted and measured outputs (over 70% correlation);

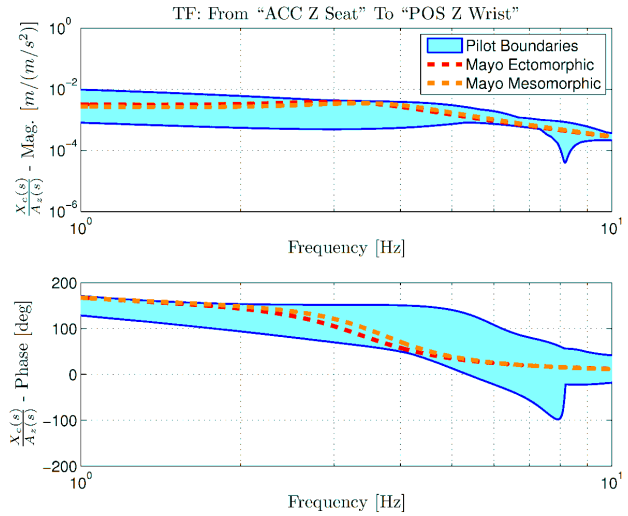


Figure 2: Identified collective BDFT transfer functions.

- the behavior of professional and ‘novice’ pilots does not show clear differences or trends; at the same time, no clear relation surfaces with pilots’ biometric measures.

According to Fig. 2, the functions identified by Mayo [6] appear to be within the identified boundaries, but the frequency of the corresponding poles, about 3.5 Hz, is lower than that of the identified ones, in the 4–5 Hz range.

2.3 Helicopter: Cyclic Control Device

In the lateral cyclic inceptor case, good coherence was observed for both measured hand acceleration and control inceptor rotation, so the two signals were used to identify separate sets of transfer functions. Key results are:

- transfer functions significantly depend on the stiffness, damping and mass of the stick; its equivalent linear stiffness is 175 N/m, the equivalent mass is 0.31612 kg and the equivalent damping is 9.0 N s/m;
- one pole at about 2–3 Hz clearly dominates the response;
- dominant poles are less damped than those of the vertical transfer functions.

Figures 3 and 4 compare the envelope of the identified functions with the function identified from data presented in [20].

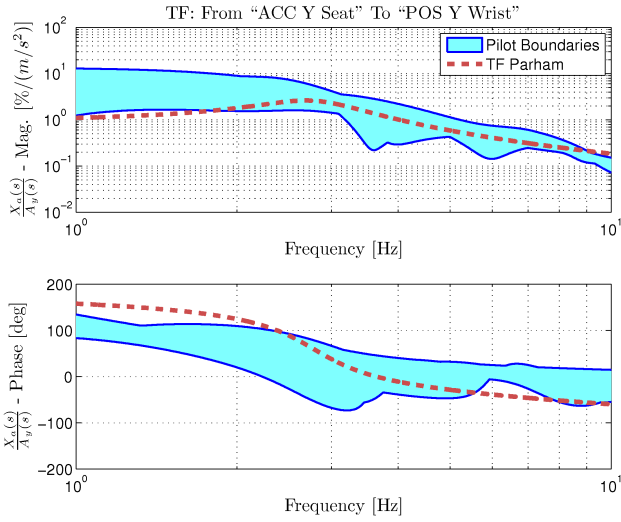


Figure 3: Identified lateral BDFT transfer functions using acceleration measures.

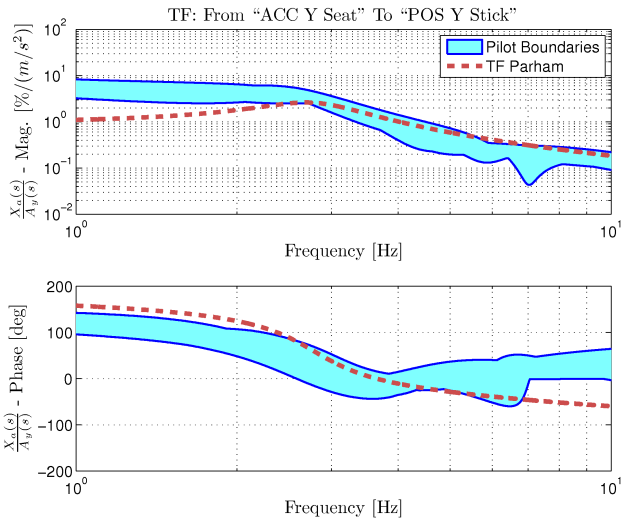


Figure 4: Identified lateral BDFT transfer functions using stick rotation measures.

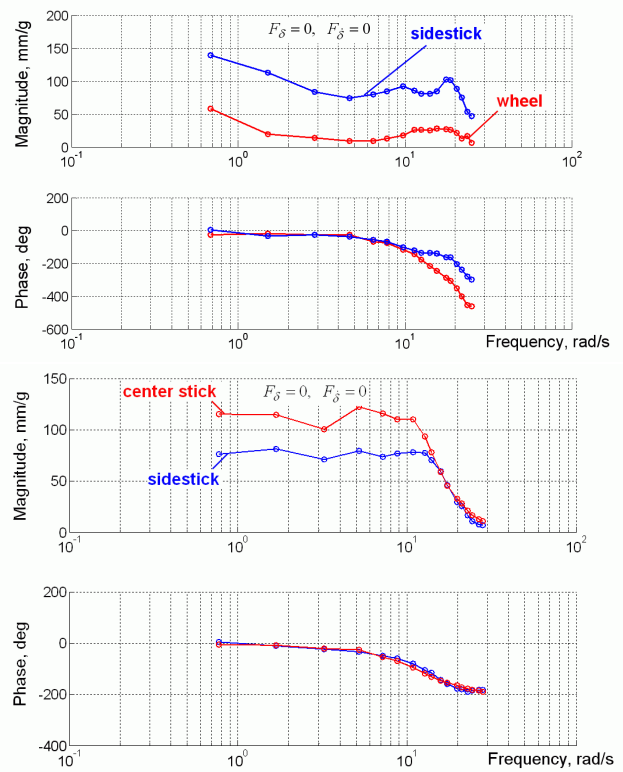


Figure 5: Effect of inceptor type.

2.4 Aircraft: Comparison of Wheel, Center Stick, and Sidestick

As it was stated in previous publications (see, for example, [21]), within a limited range of friction and breakout forces variation, the effect of breakout force on BDFT is somewhat similar to the effect of force gradient, and the effect of friction is similar to the effect of damping. Thus, we pay here the greater attention to the effect of force gradient and damping.

The type of inceptor affects BDFT intensity in a considerable extent. Figure 5 shows that BDFT tendency with a wheel is 3–4 times less than for a sidestick. For a center stick, the BDFT tendency is 2 times greater than for a sidestick. The effect of feel system characteristics on BDFT is qualitatively similar for all considered types of inceptors (center stick, wheel, sidestick). Therefore, the analysis of the feel system effect will be conducted here on the example of the sidestick, the inceptor that gained more and more popularity in recent years.

As it is seen from Fig. 6, the force gradient increase leads to BDFT tendency diminishing. To make the reduction of BDFT tendency more effective, we need to increase the force gradient more than twice as much. But this can lead to rigid-body handling quality wors-

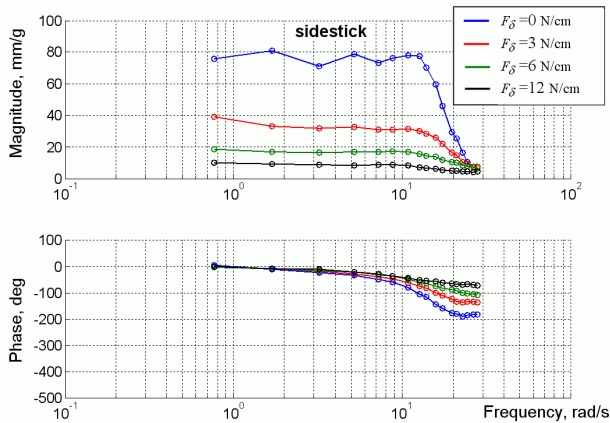


Figure 6: Effect of sidestick force gradient.

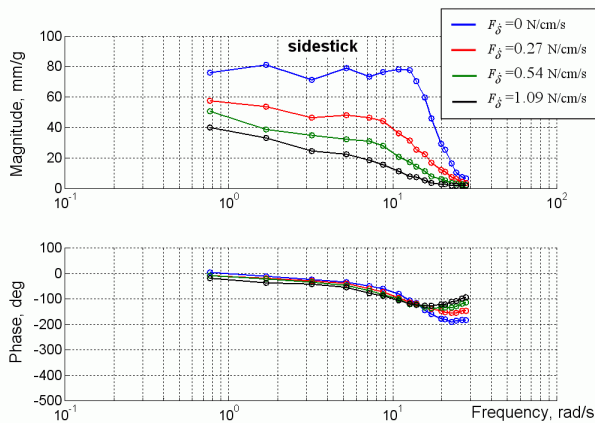


Figure 7: Effect of sidestick damping.

ening. Thus, the force gradient can not be considered an effective parameter to reduce pilot-aircraft biodynamical interaction. As inceptor damping increases, the BDFT tendency decreases noticeably, at high frequencies in particular (Fig. 7). Unlike force gradient, the variation of damping in a wide range does not lead to any noticeable changes in rigid-body HQ ratings; thus, damping can be considered an effective parameter to reduce BDFT tendency.

Summarizing the analysis, the following conclusions can be made:

- Biodynamical interaction (biodynamical pilot describing function) depends on the type of inceptor. Among the inceptors considered in the study (traditional wheel, center stick, sidestick) the BDFT is least pronounced for the wheel.
- Inceptor damping is the most effective method to suppress high-frequency oscillations, since, first, its variation in a wide range does not worsen pilot

HQ ratings, and, second, it decreases the high-frequency inceptor oscillations in a considerable extent.

Experimental data allows identification of the biomechanical model transfer function. The modern mathematical software allows identification of transfer functions of almost any complexity. The transfer function obtained in such a way is a function, whose numerator and denominator are high-order polynomials, and for any other feel system configuration new polynomials with new sets of coefficients will be obtained. However, in this case it is hardly possible to define the coefficients' adjustment rules. The procedure to define the adjustment rules appears simpler and more natural if the structure of the transfer function is predetermined and given as a set of elementary functions (aperiodic, periodic, etc.). Transfer function identification was performed based on the data obtained using GRACE (NLR) for the center and side sticks; for the wheel, the data obtained using PSPK-102 (TsAGI) were used. Comparison of the calculated and experimental describing functions showed that sufficient agreement is achieved if we use the following transfer function:

$$(3) \quad Y_{bp}(s) = K \cdot \frac{T_s + 1}{T_I s + 1} \cdot \frac{1}{T_I^2 s^2 + 2T_I \zeta_1 s + 1}$$

For the baseline set of feel system characteristics, the values of the parameters in Eq. (3) are reported in Table 1. If the feel system characteristics differ from the baseline ones (i.e. increase), the parameters of Eq. (3) change. For the sidestick, the rules of parameter adjustment are shown in Fig. 8 for force gradient and in Fig. 9 for damping. Similar functions can be calculated for a center stick and wheel.

Figure 10 confirms the validity of the identified transfer functions by their comparison with the experimental describing functions of the biodynamical pilot models.

3 MULTIBODY APPROACH

This section describes the multibody model of the biomechanics of a pilot's arm applied to the model-

Table 1: Baseline feel system characteristics, Eq. (3).

| | wheel | sidestick | center stick | |
|-----------|-------|-----------|--------------|------|
| K | 25.0 | 80.0 | 130.0 | mm/g |
| T | 0.5 | 0.5 | 1.2 | s |
| T_I | 0.8 | 0.8 | 1.2 | s |
| T_1 | 0.065 | 0.065 | 0.065 | s |
| ζ_1 | 0.5 | 0.5 | 0.8 | n.d. |



Figure 8: Transfer function parameter adjustment for the effect of inceptor force gradient.

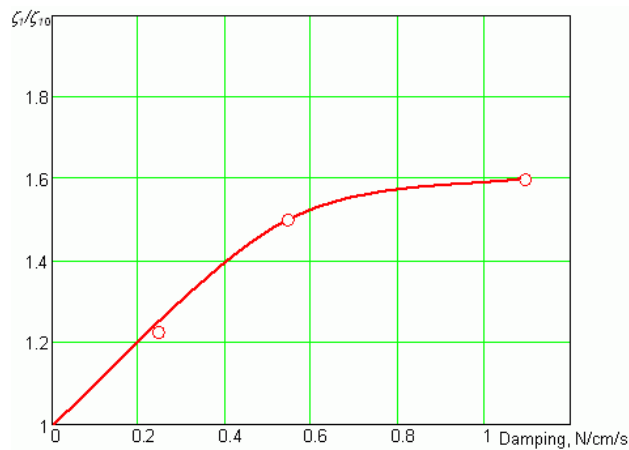
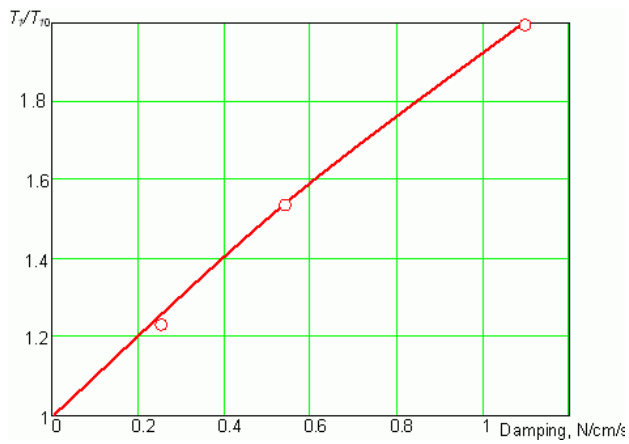


Figure 9: Transfer function parameter adjustment for the effect of inceptor damping (force gradient equal to 6 N/cm).

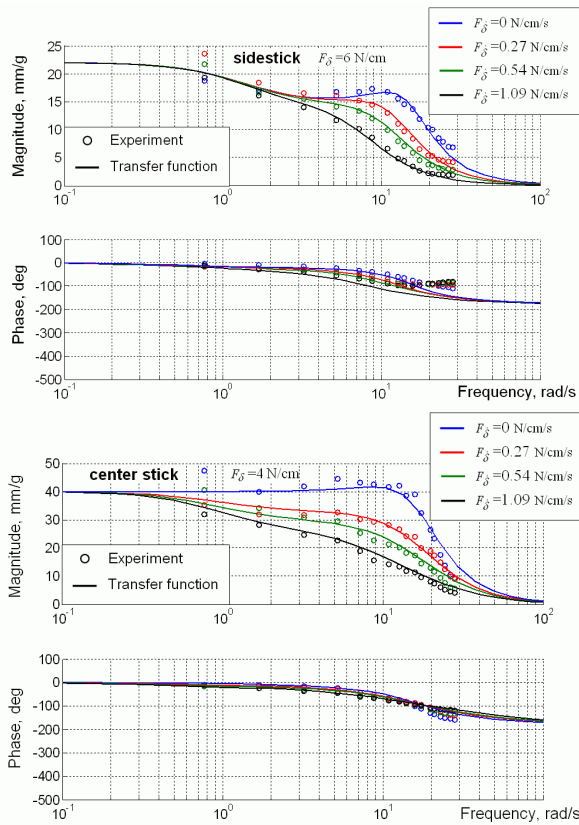


Figure 10: Agreement between the experimental and calculated describing functions for a center stick and sidestick. Effect of damping.

ing of the arm holding a conventional helicopter collective control inceptor. In [22], the problem of estimating BDFT is decomposed in a logical sequence of phases. The posture of the pilot, and specifically of his/her arms, changes while moving the control inceptors. Determining the posture of an arm when the position of shoulder and hand are at least partially prescribed is a kinematically underdetermined problem; as a consequence, a problem similar to motion planning needs to be solved. The latter can be addressed by minimizing a performance measure [22–25], or by operating on a database of trajectories collected through experiments [26]. Tracking methods produce realistic motion planning by exploiting features of measured motions; however, they need measurements specific for the motion under analysis to produce motions with both natural and subject-specific characteristics. Performance minimization heavily relies on the definition of an appropriate performance measure. Current research (e.g. [26, 27]) attempts to blend the two approaches under the expectation that measurements may improve the quality of the prediction by introducing natural and subject-specific characteristics of task execution.

The work illustrated in [22] exploits the local staggered performance minimization proposed in [28] for robotics applications, extending the approach proposed in [29]. As long as the trajectory is determined, the joint torques required to produce the desired motion, also considering the other dead loads acting on the system, are computed by solving an inverse dynamics problem.

At this point, the forces exerted by the muscles are estimated according to a simple muscle model, as functions of the required muscular activation, which accounts for the modification in muscle properties produced by the voluntary or reflexive neural stimulus that causes the contraction of the muscle. The problem of estimating muscular activation parameters is underdetermined as well; it is solved according to the *total activation* paradigm.

The proposed approach was used in [22] to develop a multibody model of a pilot’s left arm actuating a conventional collective control inceptor using the general-purpose multibody solver MBDyn². It was subsequently used in [30] to analyze BDFT between seat heave motion and collective control inceptor motion for different tasks and control configurations.

3.1 Multibody Model

The multibody model of the left arm is shown in Figure 11. It consists of rigid bodies connected by ideal

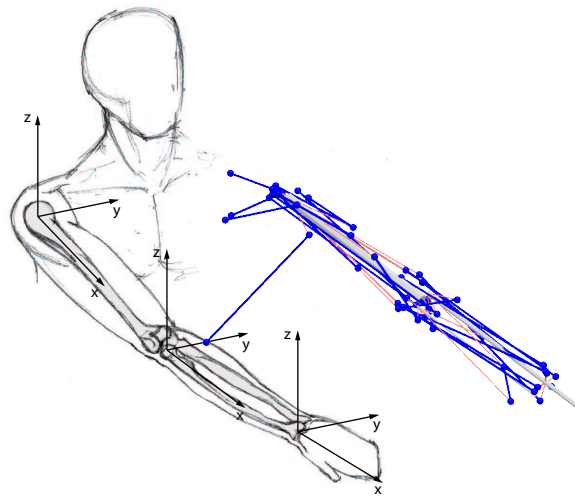


Figure 11: Multibody model of the arm.

kinematic constraints, under the assumption that the compliance of the limbs and of the articulations can be neglected at this stage, since relatively low loads and slow motions are considered.

The arm is rigidly connected to the cockpit at the shoulder. The humerus, the radius, the ulna and the hand are modeled as rigid bodies, which account for $6 \times 4 = 24$ degrees of freedom.

The articulation of the shoulder complex is modeled as a spherical hinge that prescribes the coincidence of the center of the proximal condyle of the humerus and the center of the glenoidal fossa, removing 3 degrees of freedom. A revolute hinge approximates the humeroulnar joint, allowing the ulna to rotate with respect to the humerus about its y -axis, centered in the trochlea, removing 5 degrees of freedom. The humeroradial joint is approximated by a spherical joint that prescribes the center of the capitulum to be in a point slightly outside the physical proximal end of the radius, thus removing 3 degrees of freedom. The proximal and distal radioulnar joints are approximated by a single inline joint between a point P and the mechanical x -axis of the ulna. The point P is offset from the radius axis in the local y direction in such a way that the two bones are parallel in rest position, i.e. the configuration in which the arm is full extended, pointing anteriorly, with the palm facing upward. The inline joint removes 2 degrees of freedom. A universal hinge models the carpal complex, thus allowing the flexion and the radio-ulnar deviation of the wrist, removing 4 more degrees of freedom. As a consequence, the resulting model has 7 degrees of freedom and thus its configuration would be underdetermined even in case all 6 degrees of freedom of the hand were prescribed.

²<http://www.mbdyn.org/>

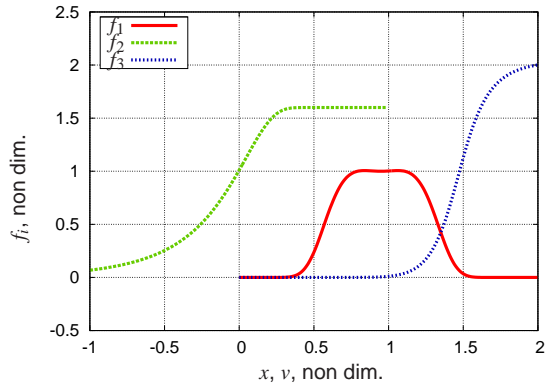


Figure 12: Non-dimensional contributions to simplified Hill's model proposed in [29].

3.2 Muscle Model

The force exerted by muscles is essentially tensile and depends on muscle length, elongation rate and activation level. The simplification of Hill's muscle force model proposed in [29] has been considered. Approximate forms of the force are developed as functions of the peak isometric force, f_0 and the reference length, l_0 ; in most applications, a fixed value of the reference velocity V_0 can be used. The tensile force exerted by the muscle is expressed as

$$(4) \quad f_m = f_0 (f_1(x)f_2(v)a + f_3(x))$$

as a function of the non-dimensional length $x = l/l_0$ and velocity $v = \dot{l}/V_0$; the force is linear in the activation parameter a , which is limited in the interval $0 \leq a \leq 1$. The non-dimensional functions f_1 , f_2 , and f_3 are shown in Figure 12.

The model considers 25 muscle bundles associated with the actuation of the articulations of the arm. Their properties are listed in Table 3 of [22]. Each muscle is modeled using a rod element that connects the related bodies at the insertion points. A special constitutive law has been implemented as a user-defined, run-time loadable module for MBDyn.

Once the torque about each joint has been computed by the inverse dynamics procedure, the muscular activation of each muscle that concurs to providing the required joint torque must be computed. The problem is underdetermined, as 7 torques are determined by the forces exerted by 25 muscles. Activations are computed minimizing their norm subjected to the constraint of producing the required torque and remaining within the $[0, 1]$ range.

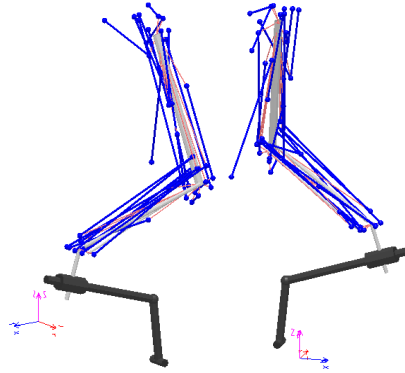


Figure 13: Sketch of the multibody model of the pilot's left arm holding the collective control inceptor.

3.3 Vertical Maneuver

The 'Aeronautical Design Standard — Performance Specification for Handling Qualities Requirements for Military Rotorcraft' (ADS-33, [31]) defines a vertical maneuver consisting in transitioning from hover in ground proximity to hover 25 ft above, and quickly returning to the initial position. The maneuver resembles the unmask/remask of scout/attack helicopters.

A similar maneuver, with focus placed on unmasking by transitioning 75 ft (22.86 m) along the heave axis, was simulated during an experimental campaign performed at the University of Liverpool within the project ARISTOTEL to investigate pilot-in-the-loop aeroelastic rotorcraft-pilot couplings [32]. The control inceptor configuration is mutated from the HELIFLIGHT flight simulator pod (see [8, 33]), which is sketched in Fig. 13 along with the multibody model of the pilot's left arm holding the collective control inceptor.

Figure 14 contains a sketch of the experimental setup and the plot of the vertical displacement of the helicopter as a consequence of the rotation of the collective control inceptor. At $t = 18$ s the collective lever is moved downwards; as a consequence, a gentle descent starts. At $t = 25$ s the collective lever is suddenly moved upwards to stop the descent, and a compensatory maneuver occurs until $t = 30$ s in order to achieve an altitude of about 0 m, as requested by ADS-33. The measures reported in Fig. 14 and used throughout this work were collected during the tests presented in [32].

When the muscular force is perturbed at fixed activation level a , the so-called 'intrinsic' stiffness is obtained [34]. This value can be very small compared to the actual stiffness that may be obtained when the effect of the reflexive system is considered. The total stiffness can be from 10 to 20 times larger, depend-

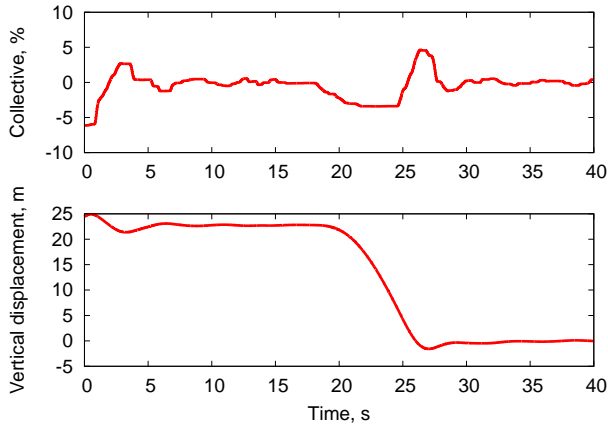


Figure 14: Collective control rotation and helicopter vertical displacement.

ing on the reference activation level [34]. This effect can be approximated expressing the perturbation of the muscular forces as

$$(5) \quad \delta \tilde{\mathbf{f}}_m = \tilde{\mathbf{f}}_{m/l} \delta \mathbf{l} + \tilde{\mathbf{f}}_{m/i} \delta \dot{\mathbf{l}} + \tilde{\mathbf{f}}_{m/a} \delta \mathbf{a},$$

where $\delta \mathbf{a}$ is associated with the reflexive system using the simple proportionality relationship

$$(6) \quad \delta \mathbf{a} = \mathbf{K}_p \text{diag}(1/l_0) \delta \mathbf{l} + \mathbf{K}_d \text{diag}(1/V_0) \delta \dot{\mathbf{l}},$$

in which \mathbf{K}_p and \mathbf{K}_d are the proportional and derivative ‘gains’. Equation (6) expresses the activation change as a consequence of a position or velocity ‘error’ as a first-order quasi-steady approximation. The perturbation of the muscular forces becomes

$$(7) \quad \delta \tilde{\mathbf{f}}_m = \left(\tilde{\mathbf{f}}_{m/l} + \tilde{\mathbf{f}}_{m/a} \mathbf{K}_p \text{diag}(1/l_0) \right) \delta \mathbf{l} + \left(\tilde{\mathbf{f}}_{m/i} + \tilde{\mathbf{f}}_{m/a} \mathbf{K}_d \text{diag}(1/V_0) \right) \delta \dot{\mathbf{l}}.$$

Figure 15 shows the collective control inceptor of a helicopter flight simulator held at 10%, 50%, and 90% of the allowed amplitude. Figure 16 shows the modification of the equivalent stiffness, damping and inertia reduced to the rotation of the collective control inceptor in the above mentioned positions. The gains of each muscle have been set to $k_p = 0.8$ and $k_d = 0.08$ to match the ratio between the total and the intrinsic stiffness and damping proposed by Stroeve [34]. The frequency and damping of the single degree of freedom system corresponding to the biodynamic feedthrough function estimated using the proposed approach are compared with the corresponding values obtained during the test campaign discussed in [8] (indicated as ‘exp, pilot #1’ and ‘exp, pilot #2’ in Fig. 16), and with data from [6] (indicated as ‘ectomorphic’ and ‘mesomorphic’). The poles of the function

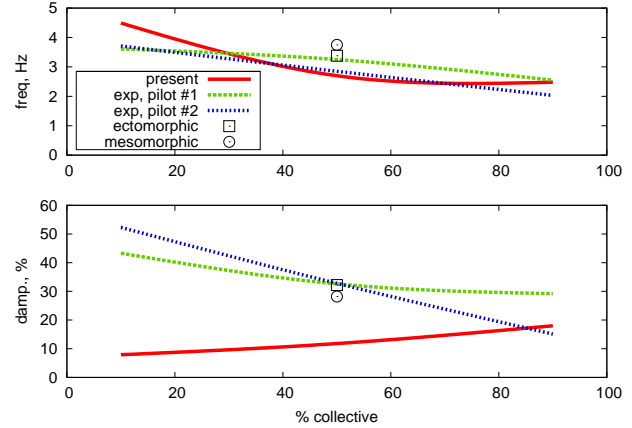


Figure 16: Frequency and damping of equivalent dynamic model vs. collective lever position.

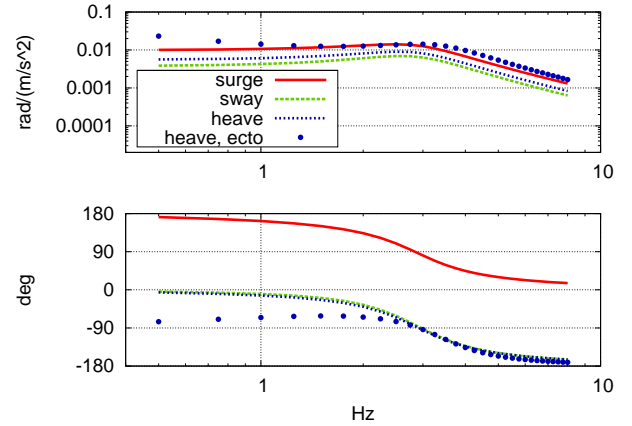


Figure 17: Collective control rotation induced by seat accelerations.

presented in [6] have been arbitrarily associated with the 50% position in the figure. The results in Fig. 16 show some common trends; for example, the predicted frequency decreases with the increase of the collective lever position, as confirmed by the experiments. However, the trend on the damping factor is incorrect. In fact the predictions indicate an increase rather than a decrease with the increase of collective lever position. The order of magnitude of the frequency was matched very well by choosing the gain k_p according to Stroeve’s results [34].

The example plots in Fig. 17 illustrate the frequency response of the collective control inceptor when the pilot’s seat is excited by accelerations in the surge (longitudinal), sway (lateral) and heave (vertical) directions. The heave plot obtained with the ectomorphic model from [6] is also shown; the non-physical low-frequency behavior should not be considered. The

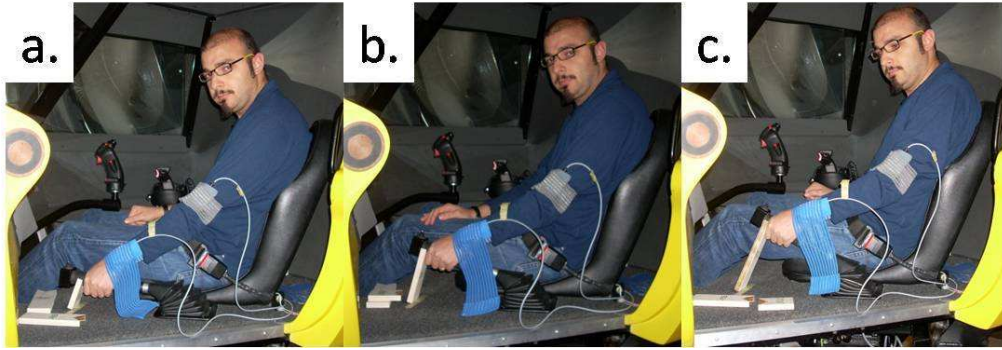


Figure 15: Experimental setup for pilot's left arm biomechanical characterization: 10% (a), 50% (b), and 90% (c) reference position of the collective control inceptor.

qualitative correlation with the present curve is good; as anticipated, the frequency of the poles resulting from the present analysis is slightly lower; moreover, the amplitude is about half that of [6]. It is interesting to notice that a significant amount of collective control rotation occurs also in response to the surge and sway motions. This cross-coupling between axes is often neglected in the literature, but it can be at least estimated using the proposed approach.

Figures 18 and 19 respectively show the BDFT and the Neuromuscular Admittance (NA) of the pilot's left arm holding the collective control inceptor in the 10%, 50% and 90% configurations, with reflexive muscular activation tuned to yield the behaviors indicated in [5] as position task (PT: the pilot tries to keep the control in the specified position), force task (FT: the pilot only provides the force required to hold the inceptor in the reference position, without trying to compensate its departure from the nominal position), and relax task (RT: intermediate between PT and FT). The plots show significant variability and, at the same time, show a qualitatively good resemblance with experimental data.

4 APPLICATIONS

4.1 Helicopters

The availability of BDFT and NA transfer functions is very important for practical applications. The Bode plots of the BDFT can be directly used to evaluate the robustness of the stability and of the performances of pilot-in-loop vehicle models, even in graphical form, as proposed for example in [35].

Transfer functions can be identified either from experiments or from the numerical BDFT and neuromuscular admittance analysis discussed in previous sections, to be used in linear/linearized analy-

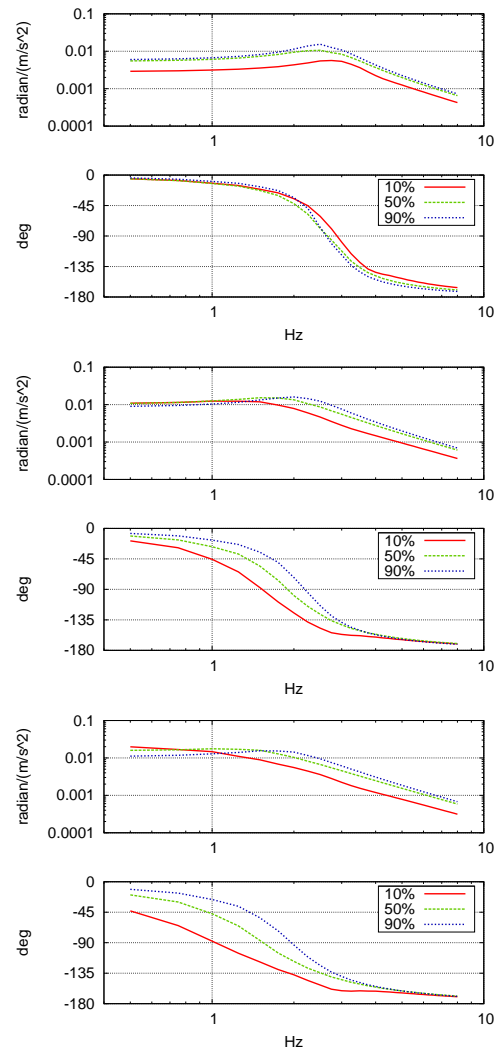


Figure 18: Collective control biodynamic feedthrough for PT (top), RT (mid) and FT (bottom) at 10%, 50%, and 90% reference collective control.

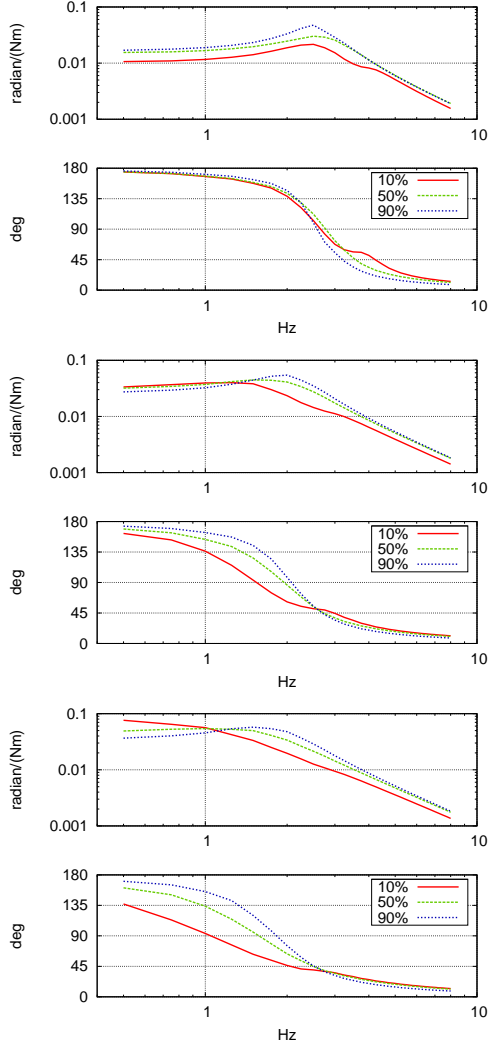


Figure 19: Collective control NA for PT (top), RT (mid) and FT (bottom) at 10%, 50%, and 90% reference collective control.

sis [15, 17, 36]. Such transfer functions can be directly used in aeroservoelastic simulations to close the vehicle control loop.

Consider for example the pilot BDFT relation

$$(8) \quad \psi = H_{\text{BDFT}}(s)s^2z,$$

where ψ is the control device rotation and z is the heave motion of the cockpit. An aeroservoelastic vehicle model of the collective bounce problem,

$$(9) \quad z = H_{z\theta}(s)\theta_0 + H_{zu}(s)u,$$

expresses z as a function of the collective pitch θ_0 and of u , a generic input/disturbance (e.g. a gust). The coupled problem is

$$(10) \quad (1 - H_{z\theta}(s)G_cH_{\text{BDFT}}(s)s^2)z = H_{zu}(s)u,$$

where G_c is the gearing ratio between the control inceptor rotation and the collective pitch, $\theta_0 = G_c\psi$.

The neuromuscular admittance function $H_{NA}(s)$ relates the device rotation angle ψ to the applied moment m . The device rotation can be expressed as

$$(11) \quad \psi = H_{NA}(s)m + H_{\text{BDFT}}(s)s^2z;$$

thus, the moment can be expressed as

$$(12) \quad m = H_{NA}^{-1}(s)(\psi - H_{\text{BDFT}}(s)s^2z)$$

and added to the equilibrium equation of the control inceptor. Laplace transform manipulation, complemented by approximation of transfer functions using rational polynomial forms as needed, can be used to express the moment as a function of ψ and z and their time derivatives also in the time domain.

Figure 20 illustrates the stability limit curves of a detailed aeroservoelastic model of a helicopter compared with experimental BDFT data, adapted from [35], to determine the stability margins with respect to the pilot's involuntary control action, treated as the uncertain element in a control loop. The interaction may lead to instability when the phase curves cross and, at the same time, the amplitude of the BDFT is above the limit (solid curve). In the figure, this can only occur with PT, at about 3.5 Hz (shaded regions represent 1, 2 and 3 sigma deviations with respect to the mean value, indicated by the solid line).

Detailed analysis of collective bounce using linearized comprehensive models and detailed nonlinear multibody models of helicopters including the biomechanics of the pilot are presented for example in [13, 17, 22, 36, 37].

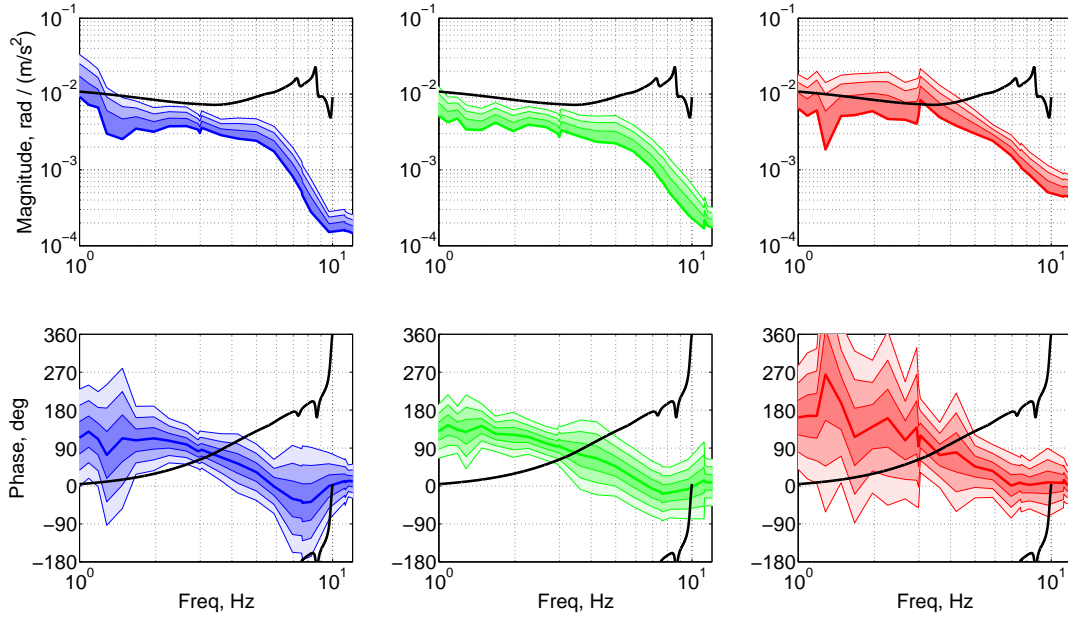


Figure 20: Magnitude and phase stability limits of aeroservoelastic helicopter model in hover (solid line) and pilot BDFT according to FT (left), RT (center) and PT (right).

4.2 Fixed Wing Aircraft

The availability of biomechanical models allows developing HQ criterion for flexible aircraft, which would take into account aircraft structural elasticity characteristics and inceptor feel system characteristics.

The main idea of the criterion is that the worsening of aircraft handling qualities, caused by biodynamical effect of elastic oscillations, is determined by parameter λ : $\Delta PR = \Delta PR(\lambda)$, where $\lambda = \sigma_{n_y} / \sigma_p$. In this expression, σ_{n_y} is the RMS of the lateral accelerations due to biodynamical interaction, σ_p is the RMS of the deliberately created roll rates.

The transfer function for the biodynamical interaction of Eq. (3) will be used in the criterion to calculate σ_{n_y} in accordance with the following expression:

$$(13) \quad \sigma_{n_y}^2 = \frac{1}{2\pi} \int_{-\infty}^{\infty} |Y_{n_y}(j\omega) \cdot Y_{bp}(j\omega)|^2 d\omega$$

where Y_{n_y} is transfer function for the lateral accelerations of the elastic aircraft, Y_{bp} is transfer function of the biomechanical interaction for the particular inceptor type and its feel system characteristics. In greater details, the description of the criterion will be made in the next publications.

5 CONCLUSIONS

This work presented experimental and numerical results of biodynamic feedthrough related to fixed and rotary wing aircraft. Several experiments have been conducted in relation with conventional helicopter collective and lateral cyclic control inceptors in the flight simulator to characterize the biomechanical behavior of the pilot. A considerable variability has been observed between the tested subjects and also within each subject for varied test conditions. Envelopes of biodynamic feedthrough have been estimated, which reasonably correlate with data from the existing open literature. Furthermore, a detailed biomechanical model of the pilot's arm has been developed within a multibody dynamics modeling environment. The model has been used to predict biodynamic feedthrough and neuromuscular admittance frequency response and also to perform direct bioaeroservoelastic simulations of the helicopter that include the pilot's biodynamics. The model was able to qualitatively predict the dependence of biodynamic feedthrough on the cockpit layout and on the posture of the pilot, and also the dependence of biodynamic feedthrough on the task the pilot is required to perform by empirically acting on an intuitive approximation of the reflexive muscular activation.

The analysis of the biodynamical test results on the

effect of different inceptor types and feel system characteristics on BDFT showed that:

- biodynamical interaction (biodynamical pilot model) depends on inceptor type: the smallest BDFT is observed for the wheel, whereas the largest BDFT is observed for a center stick;
- inceptor damping is the most effective method to suppress biodynamical interaction, since it considerably reduces the high-frequency inceptor oscillations and, at the same time, does not cause pilot ratings deterioration in a wide range of its variation.

On the basis of the BDFT experimental describing functions, identification is made of the biomechanical model transfer function, and the rules of its parameter adjustment are determined as a function of force gradient and damping for all considered types of inceptors. The conducted analysis and the identified transfer function will be used to develop criteria to assess the effect of aircraft structural elasticity with regard to inceptor feel system characteristics.

ACKNOWLEDGMENTS

The research leading to these results has received funding from the European Community's Seventh Framework Programme (FP7/2007-2013) under grant agreement N. 266073.

REFERENCES

- [1] Raymond E. Magdaleno, Duane T. McRuer, and George P. Moore. Small perturbation dynamics of the neuromuscular system in tracking tasks. CR 1212, NASA, 1968. TR-154-1.
- [2] Raymond E. Magdaleno and Duane T. McRuer. Experimental validation and analytical elaboration for models of the pilot's neuromuscular subsystem in tracking tasks. CR 1757, NASA, 1971.
- [3] Henry R. Jex and Raymond E. Magdaleno. Biomechanical models for vibration feedthrough to hands and head for a semisupine pilot. *Aviation, Space, and Environmental Medicine*, 49(1–2):304–316, 1978.
- [4] Gordon Höhne. A biomechanical pilot model for prediction of roll ratcheting. In *AIAA Atmospheric Flight Mechanics Conference*, Portland, OR, USA, August 9–11 1999. AIAA-1999-4092.
- [5] J. Venrooij, D. A. Abbink, M. Mulder, M. M. van Paassen, and M. Mulder. Biodynamic feedthrough is task dependent. In *2010 IEEE International Conference on Systems Man and Cybernetics (SMC)*, pages 2571–2578, Istanbul, Turkey, October 10–13 2010. doi:10.1109/ICSMC.2010.5641915.
- [6] John R. Mayo. The involuntary participation of a human pilot in a helicopter collective control loop. In *15th European Rotorcraft Forum*, pages 81.1–12, Amsterdam, The Netherlands, 12–15 September 1989.
- [7] M. Jump, S. Hodge, B. DangVu, P. Masarati, G. Quaranta, M. Mataboni, M. D. Pavel, and O. Dieterich. Adverse rotorcraft-pilot coupling: Test campaign development at the university of Liverpool. In *34th European Rotorcraft Forum*, Liverpool, UK, September 16–19 2008.
- [8] Pierangelo Masarati, Giuseppe Quaranta, and Michael Jump. Experimental and numerical helicopter pilot characterization for aeroelastic rotorcraft-pilot couplings analysis. *Proc. IMechE, Part G: J. Aerospace Engineering*, 227(1):124–140, January 2013. doi:10.1177/0954410011427662.
- [9] Marilena D. Pavel, Jacek Malecki, Binh DangVu, Pierangelo Masarati, Massimo Gennaretti, Michael Jump, Michael Jones, Hafid Smaili, Achim Ionita, and Larisa Zaicek. Present and future trends in aircraft and rotorcraft pilot couplings — a retrospective survey of recent research activities within the European project ARISTOTEL. In *37th European Rotorcraft Forum*, Gallarate, Italy, September 13–15 2011. Paper no. 116.
- [10] Marilena D. Pavel, Jacek Malecki, Binh DangVu, Pierangelo Masarati, Massimo Gennaretti, Michael Jump, Hafid Smaili, Achim Ionita, and Larisa Zaicek. A retrospective survey of adverse rotorcraft pilot couplings in European perspective. In *American Helicopter Society 68th Annual Forum*, Fort Worth, Texas, May 1–3 2012.
- [11] Marilena D. Pavel, Michael Jump, Binh Dang-Vu, Pierangelo Masarati, Massimo Gennaretti, Achim Ionita, Larisa Zaichik, Hafid Smaili, Giuseppe Quaranta, Deniz Yilmaz, Michael Jones, Jacopo Serafini, and Jacek Malecki. Adverse rotorcraft pilot couplings — past, present and future challenges. *Progress in Aerospace Sciences*, In Press, Available online 4 July 2013.
- [12] Michael Jones, Michael Jump, Linghai Lu, Deniz Yilmaz, Marilena D. Pavel, Pierangelo Masarati, Giuseppe Quaranta, and Vincenzo Muscarello. The role of flight simulation in exposing rotorcraft pilot couplings. In *39th European Rotorcraft Forum*, Moscow, Russia, September 3–6 2013.
- [13] Massimo Gennaretti, Marco Molica Colella, Jacopo Serafini, Binh DangVu, Pierangelo Masarati, Giuseppe Quaranta, Vincenzo Muscarello, Michael Jump, Michael Jones, Achim Ionita, Ion Fuiorea, Mihai Mihaila-Andres, and Stefan Radu. Anatomy, modelling and prediction of aeroservoelastic rotorcraft-pilot-coupling. In *39th European Rotorcraft Forum*, Moscow, Russia, September 3–6 2013.
- [14] V. V. Rodchenko, L. E. Zaichik, and Y. P. Yashin et. al. Investigation of controllability criteria of class III aircraft equipped with a sidestick. Technical Report WL-TR-96-3079, Wright-Patterson Laboratory, December 1994.
- [15] O. Dieterich, J. Götz, B. DangVu, H. Haverdings, P. Masarati, M. D. Pavel, M. Jump, and M. Gennaretti. Adverse rotorcraft-pilot coupling: Recent research activities in Europe. In *34th European Rotorcraft Forum*, Liverpool, UK, September 16–19 2008.
- [16] M. D. Pavel, B. DangVu, J. Götz, M. Jump, and O. Dieterich. Adverse rotorcraft-pilot coupling: Prediction and suppression of rigid body RPC. In *34th European Rotorcraft Forum*, Liverpool, UK, September 16–19 2008.
- [17] J. Serafini, M. Gennaretti, P. Masarati, G. Quaranta, and O. Dieterich. Aeroelastic and biodynamic modeling for stability analysis of rotorcraft-pilot coupling phenomena. In *34th European Rotorcraft Forum*, Liverpool, UK, September 16–19 2008.
- [18] Anonymous. Rotorcraft flying handbook. FAA H-8083-21, Federal Aviation Administration, 2000.
- [19] R. B. Blackman and J. W. Tukey. *The measurement of power spectra from the point of view of communication engineering*. Dover Publications, 1958.

- [20] T. Parham, Jr., David Popelka, David G. Miller, and Arnold T. Froebel. V-22 pilot-in-the-loop aeroelastic stability analysis. In *American Helicopter Society 47th Annual Forum*, Phoenix, Arizona (USA), May 6–8 1991.
- [21] L. E. Zaichik, P. A. Desyatnik, K. N. Grinev, and Y. P. Yashin. Effect of manipulator type and feel system characteristics on high-frequency biodynamic pilot-aircraft interaction. In *ICAS 2012*, Brisbane, Australia, 2012. paper no. 285.
- [22] Pierangelo Masarati, Giuseppe Quaranta, and Andrea Zaroni. Dependence of helicopter pilots' biodynamic feedthrough on upper limbs' muscular activation patterns. *Proc. IMechE Part K: J. Multi-body Dynamics*, in press. doi:10.1177/1464419313490680.
- [23] Yujiang Xiang, Hyun-Joon Chung, Joo H. Kim, Rajankumar Bhatt, Salam Rahmatalla, Jingzhou Yang, Timothy Marler, Jasbir S. Arora, and Karim Abdel-Malek. Predictive dynamics: an optimization-based novel approach for human motion simulation. *Structural and Multidisciplinary Optimization*, 41(3):465–479, 2010. doi:10.1007/s00158-009-0423-z.
- [24] Yujiang Xiang, Jasbir S. Arora, Salam Rahmatalla, Timothy Marler, Rajankumar Bhatt, and Karim Abdel-Malek. Human lifting simulation using a multi-objective optimization approach. *Multibody System Dynamics*, 23(4):431–451, 2010. doi:10.1007/s11044-009-9186-y.
- [25] Yujiang Xiang, Jasbir S. Arora, Hyun-Joon Chung, Hyun-Jung Kwon, Salam Rahmatalla, Rajankumar Bhatt, and Karim Abdel-Malek. Predictive simulation of human walking transitions using an optimization formulation. *Structural and Multidisciplinary Optimization*, 45(5):759–772, 2012. doi:10.1007/s00158-011-0712-1.
- [26] Yujiang Xiang, Jasbir S. Arora, and Karim Abdel-Malek. Hybrid predictive dynamics: a new approach to simulate human motion. *Multibody System Dynamics*, 28(3):199–224, 2012. doi:10.1007/s11044-012-9306-y.
- [27] I. Pasciuto, A. Valero, S. Ausejo, and J. T. Celigüeta. A hybrid dynamic motion prediction method with collision detection. In *Proc. First International Symposium on Digital Human Modeling*, 2011.
- [28] Pierangelo Masarati. Computed torque control of redundant manipulators using general-purpose software in real-time. *Multibody System Dynamics*, in press. doi:10.1007/s11044-013-9377-4.
- [29] E. Pennestri, R. Stefanelli, P. P. Valentini, and L. Vita. Virtual musculo-skeletal model for the biomechanical analysis of the upper limb. *Journal of Biomechanics*, 40(6):1350–1361, 2007. doi:10.1016/j.jbiomech.2006.05.013.
- [30] Pierangelo Masarati and Giuseppe Quaranta. Coupled bioaeroservoelastic rotorcraft-pilot simulation. In *Proceedings of ASME IDETC/CIE*, Portland, OR, August 4–7 2013. DETC2013-12035.
- [31] Anonymous. Performance specification, handling qualities requirements for military rotorcraft. ADS 33-E-PRF, US Army AMCOM, Redstone, Alabama, 2000.
- [32] Pierangelo Masarati, Giuseppe Quaranta, Linghai Lu, and Michael Jump. Theoretical and experimental investigation of aeroelastic rotorcraft-pilot coupling. In *American Helicopter Society 68th Annual Forum*, Fort Worth, Texas, May 1–3 2012.
- [33] G. D. Padfield and M. D. White. Flight simulation in academia; HELIFLIGHT in its first year of operation. *The Aeronautical Journal of the Royal Aeronautical Society*, 107(1075):529–538, September 2003.
- [34] Sybert Stroeve. Impedance characteristics of a neuromusculoskeletal model of the human arm I. posture control. *Biological Cybernetics*, 81(5–6):475–494, 1999. doi:10.1007/s004220050577.
- [35] Giuseppe Quaranta, Pierangelo Masarati, and Joost Venrooij. Impact of pilots' biodynamic feedthrough on rotorcraft by robust stability. *Journal of Sound and Vibration*, 332(20):4948–4962, September 2013. doi:10.1016/j.jsv.2013.04.020.
- [36] Massimo Gennaretti, Jacopo Serafini, Pierangelo Masarati, and Giuseppe Quaranta. Effects of biodynamic feedthrough in rotorcraft-pilot coupling: the collective bounce case. *J. of Guidance, Control, and Dynamics*, to be published. doi:10.2514/1.61355.
- [37] Pierangelo Masarati, Giuseppe Quaranta, Massimo Gennaretti, and Jacopo Serafini. An investigation of aeroelastic rotorcraft-pilot interaction. In *37th European Rotorcraft Forum*, Gallarate, Italy, September 13–15 2011. Paper no. 112.

COPYRIGHT STATEMENT

The authors confirm that they, and/or their company or organization, hold copyright on all of the original material included in this paper. The authors also confirm that they have obtained permission, from the copyright holder of any third party material included in this paper, to publish it as part of their paper. The authors confirm that they give permission, or have obtained permission from the copyright holder of this paper, for the publication and distribution of this paper as part of the ERF2013 proceedings or as individual offprints from the proceedings and for inclusion in a freely accessible web-based repository.